The Building Blocks of Metallothioneins: Heterometallic Zn(2+) and Cd(2+) clusters from first-principles calculations.

Kepp, Kasper Planeta; Rykær, Martin

Published in:
Dalton Transactions (Print Edition)

Link to article, DOI:
10.1039/c0dt00087f

Publication date:
2010

Document Version
Publisher's PDF, also known as Version of record

The building blocks of metallothioneins: heterometallic Zn^{2+} and Cd^{2+} clusters from first-principles calculations†

Kasper P. Jensen* and Martin Rykær

Received 8th March 2010, Accepted 16th July 2010
DOI: 10.1039/c0dt00087f

Electronic structures of Zn^{2+} and Cd^{2+} thiolate clusters found in metallothioneins (MT) have been obtained using density functional theory. We have found that the inherent asymmetry of cluster architectures gives rise to seven distinct metal sites. Whereas the non-strained bond lengths of such tetrathiolate complexes are found to be 2.60 Å and 2.39 Å for Cd–S and Zn–S, in the MT clusters four characteristic terminal and bridging bonds are observed with average lengths 2.55 Å (Cd–S^t); 2.35 Å (Zn–S^t); 2.62 Å (Cd–S^b); and 2.42 Å (Zn–S^b). For each stoichiometry of Zn^{2+} and Cd^{2+}, all possible isomers have been characterized and ranked according to relative free energy and metal ion selectivity. The most stable distribution at low Cd^{2+} concentration is computed to be $Zn_4 + CdZn_2$, whereas at 2 : 1 Cd^{2+} : Zn^{2+} concentration, only heteroclusters are thermodynamically stable, explaining experimental data. The presence of two different clusters in MTs must and can be rationalized already in their intrinsic differences. The results indicate that the asymmetry allows for Zn^{2+} transfer to various molecular targets having different thresholds for Zn^{2+} binding, while maintaining detoxification sites.

Introduction

Metallothioneins (MT) are a class of small, cysteine-rich proteins that bind metal ions such as Cd^{2+}, Cu^{+}, and Zn^{2+} *in vivo*.[1,2,3] In humans, four isoforms are usually distinguished, with MT-1 and MT-2 present in most tissue, whereas MT-3 and MT-4 appear mainly in specialized tissue such as the brain.[1] In MT-1 and MT-2, Zn^{2+} is the dominating metal bound, with some amounts of Cd^{2+} and other metal ions found as well, whereas in MT-3 found in the brain, copper and zinc are both present in significant amounts.[4]

MTs are involved in the metal-dependent cellular trafficking and signaling.[4] The main roles include transport, storage, and concentration regulation of essential metal ions;[5] detoxification of heavy metals;[6] reduction of inflammation;[7] and anti-stress function, *e.g.* in relation to oxidative stress.[8] Many of these functions rely on the ability of MTs to maintain the free intracellular concentration of Zn^{2+} low,[5,9] while supplying Zn^{2+} to various targets within the cells, *e.g.* the many Zn^{2+}-dependent enzymes,[10,11] zinc-finger dependent transcription factors,[12,13] and zinc-containing pre-synaptic vesicles in zinc-containing neurons, for maintaining synaptic activity.[14,15] The role of MTs as the main Zn^{2+} buffering proteins in the organism is emerging.[16] Thus, molecular structure–function correlations of MTs are desirable.

The various MT apoproteins tend to be disordered, but upon binding of metal ions, they take up characteristic 3-dimensional structures with similar folds.[1,17,18,19] This similarity of protein folds is accompanied by a similar composition and stoichiometry of the metal clusters.[5] With the abundance of MTs in all animals[20] these observations point towards the functional importance of this particular molecular architecture. Specifically, the mammal MTs consist of two subunits, each containing a metal-binding cluster (see Fig. 1): the α-subunit contains the A-cluster with 11 cysteines that usually bind four metal ions. The β-subunit contains the B-cluster with nine cysteines that usually binds three metal ions.[21] Thus, the normal stoichiometry is seven divalent metal ions per protein.[3]

While only a few structure–function correlations and modern electronic structure calculations have so far been achieved for MTs, cluster structures have previously been compared with inorganic model compounds containing metal–thiolate bonds.[20] These comparisons have shown that the MT clusters are distorted compared to non-strained tetrahedral geometries (see Fig. 2).[5,20] The functional significance of such distorted coordination sites is not known. In particular, since the isolated full clusters have not been synthesized, it is not clear whether this asymmetry is inherent to the clusters or due to the apoprotein.

Various chemical modifications are known to disrupt the function of MTs: the binding of metal ions to MTs is pH-dependent, most likely due to protonation of the cysteines below pH = 4.[5,22] At low pH or during oxidative stress, chemical modification of

Technical University of Denmark, DTU Chemistry, Kemitorvet 206, DK 2800, Kongens Lyngby, Denmark. E-mail: kpj@kemi.dtu.dk

† Electronic supplementary information (ESI) available: Table S1: the effect of COSMO dielectricity constants on the M–S bond lengths of thiolate complexes (data used in Fig. 3). Table S2: optimized non-screened equilibrium bond lengths of all studied isomers of $Cd_xZn_{4-x}S_{11}^{3-}$. Table S3: optimized screened equilibrium bond lengths of all studied isomers of $Cd_xZn_{4-x}S_{11}^{3-}$, screened with Cosmo model, $\varepsilon = 10$. Table S4: optimized equilibrium bond lengths of all studied isomers of $Cd_yZn_{3-y}S_9^{3-}$ (pm), screened with Cosmo model, $\varepsilon = 10$. Table S5: average equilibrium bond lengths (Å) of geometry-optimized clusters without screening. Table S6: optimized equilibrium S–M–S angles of all studied isomers, screened with Cosmo model, $\varepsilon = 10$. Table S7: mean absolute deviation (MAD) of cluster S–M–S angles from 109.5°. Table S8: "angular energies" (summed squared angular deviations from 109.5°) of clusters. Table S9: computed electronic energy, zero point energy + $3RT$, and thermodynamic state functions (thermal energy, enthalpy, entropy, and Gibbs' free energy) at 298 K (TPSSh, def-TZVP). Table S10: computed volumes and areas of cluster cavities, from Cosmo (in atomic units). Table S11: deviation from non-strained metal–sulfur bond lengths (Å). Table S12: computed atomic charges of isomers, derived from Mulliken population analysis. Table S13: bond orders (computed overlap populations × 2), derived from Mulliken analysis. Fig. S1: bond energies of metal–sulfur bonds in Cd_3 and Zn_3 clusters. See DOI: 10.1039/c0dt00087f

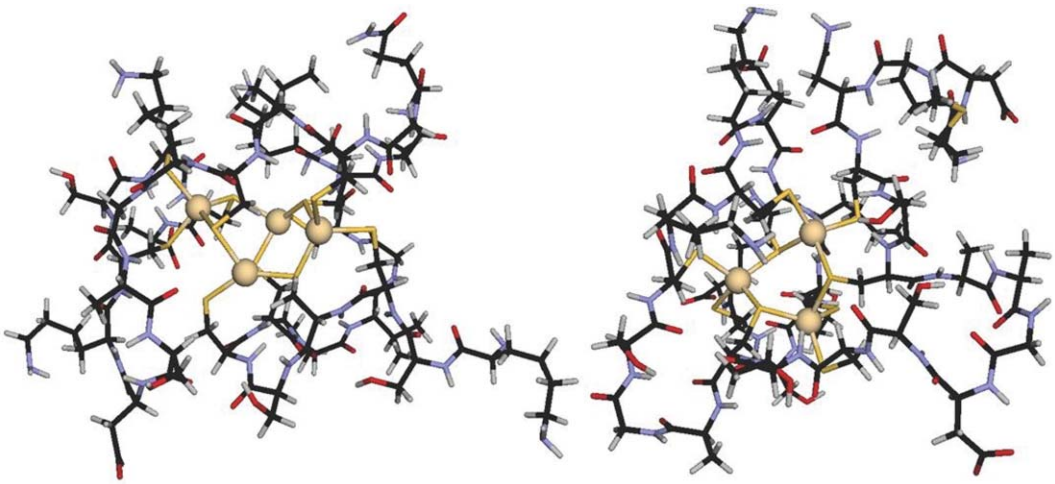

Fig. 1 Human Cd_7MT-2. Left: α-Subunit (1MHU.pdb). Right: β-Subunit (2MHU.pdb). Ref. 27.

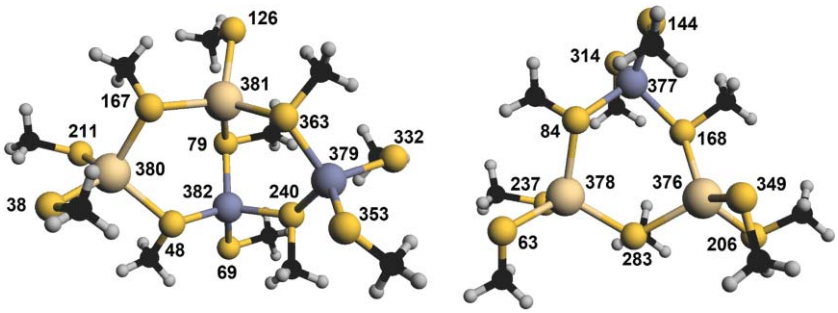

Fig. 2 Examples of geometry-optimized models used in this work. Left: the cluster A model $Cd_xZn_{4-x}S_{11}^{3-}$. Right: the cluster B model $Cd_yZn_{3-y}S_9^{3-}$.

thiolates (protonation or oxidation, respectively) may lead to loss of metal ions, and binding of unnatural metal ions may also affect structure and function. At normal physiological conditions, cysteines are deprotonated as observed in experimental structures with Zn–S bond lengths of ~2.3 Å; protonation of cysteine will increase the Zn–S bond length by 0.4 Å[23] and most likely cause metal ion dissociation.

To understand biological regulation of Zn^{2+} by MTs, one must investigate how Zn^{2+} binds to MT and how this binding is chemically modified. One common modification is binding of the rival metal ion, Cd^{2+}. Cd^{2+} is almost exclusively found in the body bound to MT and excreted *via* the kidneys.[24,25] A MT structure containing both Cd^{2+} and Zn^{2+} has been published.[26] Human MT-2 is the only human MT where structures (of the Cd_7-form) are available for both cluster A and B.[27] The presence of Cd^{2+} in MTs clearly warrants further studies in order to understand how exposure affects the function of MTs.

In order to understand the molecular function of MT, one must know whether the biologically relevant structures are under thermodynamic or kinetic control. The kinetic lability of the metal ions in MTs is relatively high,[28] implying that thermodynamic control, *i.e.* concentrations and binding affinities, dominate the chemical composition of MTs at any time. This is reasonable since concentration control (homeostasis) is a main role of these proteins. Therefore, we argue that identifying the most thermodynamically stable structures among the multitude of structures possible is equivalent to identifying the functional states of MTs. Some association constants of Zn^{2+} and Cd^{2+} binding to MTs are experimentally available.[29,30] The stabilities of human Zn_7–MTs are as follows: four Zn^{2+} ions are bound with log$K$ ~11.8, two with log$K$ ~10.0, and one with log$K$ ~7.7.[31,32]

According to some reports, the Zn_6–MT form, but not the fully loaded Zn_7–MT is observed *in vivo*,[4] making room for Cd^{2+} which binds more strongly:[31] the stability constant of Cd_7–MT2 is 3×10^{17}, or 10^4 times higher than for Zn_7–MT2,[33] *i.e.* as soon as Cd^{2+} is available, the fully loaded Cd_xZn_{7-x} forms prevail. However, in other reports, since Zn_7–MT2 is very stable with a stability constant of 3×10^{13} M^{-1},[34] it is assumed that metal substitution happens by direct substitution of another metal ion, always having fully loaded stoichiometries at normal physiological conditions. Regardless of whether the substitution for Cd^{2+} occurs *via* the Zn_6–MT intermediate or not, the thermodynamic stability of any Cd_xZn_{7-x} form determines whether this form occurs. In these cases, it is known that heteroclusters form by inter-protein metal exchange, but the reasons for the stability of the heteroclusters are not known.[35]

Only a few previous DFT[36,37] and classical force field[38] modeling studies have addressed MT structure–function correlations. Such studies have hitherto been limited to single structures (not the multitude of possible isomers and compositions). Force field methods have standards errors of at least ~0.1 Å per metal–sulfur bond and lack the details of electronic structure, whereas the standard error of DFT (BP86) is ~0.03 Å from a large data set of computed and experimental metal-ligand bond

lengths.[39] Specifically, Cd–S and Zn–S bonds have been studied in detail in recent work using various DFT functionals[40,41] to provide consistent benchmarks of this accuracy. Isomorphous substitution reactions where overall structure is retained are ideally studied by computational chemistry, since the protein will provide an almost constant field beyond the second coordination sphere.

We describe here the electronic structures of inorganic MT clusters without protein available, using the current state-of-the-art functional TPSSh, to investigate whether their unusual asymmetric geometries are inherent to the clusters or only due to the protein scaffold. The many modifications possible with Cd^{2+} have also been studied to understand whether this asymmetry gives rise to metal selectivity already at the cluster level. Even without the protein available, the clusters display highly asymmetric coordination environments with angularly distorted pseudo-tetrahedral geometries that give rise to seven distinct and unique sites. Thus, a large number of possible isomers are identified for various Cd^{2+} loads in both cluster types A and B. These isomers are characterized structurally and energetically, and their implications are discussed.

Methods

1. Computational details

Calculations were performed with the Turbomole 5.9 software.[42] Geometries were optimized using the BP86 functional,[43,44] with energies converged down to 10^{-6} hartree, and the gradient converged down to 10^{-3} a.u. The basis set used for geometry optimization was def-SVP by Schafer *et al.*[45] To model the core of Cd^{2+}, we used the standard 28-electron ecp (def-ecp) of Turbomole. This procedure is known to give accurate geometries of metal clusters, also involving Zn, Cd, and bonds to sulfur,[40,41] with mean absolute errors of ~0.03 Å in metal–ligand bonds.

During optimization, the Cosmo solvation model[46,47] with a dielectric constant of 10 was applied, to mimic real condense phase electrostatic screening in the protein ($\varepsilon \sim 4$–16),[48] in accordance with its known effect on the geometries of charged clusters.[49] In the protein, electrostatic effects are hard to measure, but some degree of condense-phase shielding is necessarily present.[23] Screening reduces the repulsion between the lone pairs of the thiolates and allows the metal–sulfur bonds to shorten by ~0.02–0.03 Å (see Fig. 3 and Tables S1–S6, ESI†), although keeping the relative length of the different types of bonds intact. Importantly, any value of ε beyond 6 has a modest effect on structure (*vide infra*), so condense-phase electrostatic screening can be modeled consistently.

All energies were recomputed after geometry optimization using the def-TZVP basis set[50] with the meta hybrid TPSSh functional.[51,52] The def-TZVP basis set is triple-zeta contracted with diffuse functions necessary for modeling anionic clusters, *e.g.* 4s3p2d1f for C/N/O.[50] For the Zn_4 structures, the total number of primitive and contracted basis functions used were 1765 and 1235, respectively, and slightly less for other structures. Any quantum-chemical study on anionic clusters using a DZP-type basis set for energies will exhibit substantial errors because of the inability to describe the radial electron correlation; diffuse functions remedy this problem.

The main reasons for using TPSSh are: (i) the TPSSh functional is non-empirical except for the $a = 0.1$ coefficient of exact exchange,

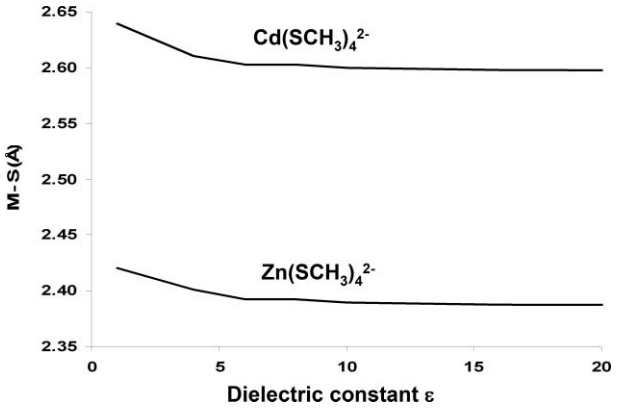

Fig. 3 Non-strained Cd–S and Zn–S bond lengths from computed $[M(SCH_3)_4]^{2-}$ models: Sensitivity to the dielectric constant ε.

implying that it does not rely on the additional parameters optimized empirically for other functionals such as B3LYP and BP86; (ii) the functional does not suffer from self interaction errors; (iii) the functional has provided the most accurate description of a variety of chemical processes involving transition metals in several benchmark studies.[40,41,53]

Zero-point energies and free energy corrections were calculated from geometry optimization and subsequent harmonic frequency and thermodynamic analysis, using the freeh script of Turbomole.

2. Chemical models

This work examines the inorganic clusters without protein, to evaluate structure and properties inherent to the cluster architectures themselves. The models were constructed from the α- and β-subunits of human Cd_7–MT2 (1MHU.pdb and 2MHU.pdb, respectively).[27] Metal ions were changed manually to generate all possible isomers and compositions possible with Zn^{2+} and Cd^{2+}, under the constraint of having all seven sites occupied. The clusters were truncated at the β-carbons of the cysteines, and hydrogen was added in place of the α-carbons. Examples of these models are shown in Fig. 2. The atom numbers correspond to the numbers in the published pdb files.

All reactions studied here are isodesmic, *i.e.* do not change the number and types of chemical bonds. Specifically, the number of Cd–S and Zn–S bonds are preserved in all studied reactions. Examples include isomerization reactions such as eqn (1):

$$[Cd_mZn_{4-m}(SCH_3)_{11}]_K^{3-} \rightarrow [Cd_mZn_{4-m}(SCH_3)_{11}]_L^{3-} \quad (1)$$

Here, *K* and *L* denote distinct isomers of the same composition of an A-cluster; or metal exchange reactions such as eqn (2):

$$[Cd_mZn_{4-m}(SCH_3)_{11}]^{3-} + [Cd_nZn_{4-n}(SCH_3)_{11}]^{3-} \rightarrow [Cd_{m+1}Zn_{3-m}(SCH_3)_{11}]_L^{3-} + [Cd_{n-1}Zn_{5-n}(SCH_3)_{11}]^{3-} \quad (2)$$

This is a Cd/Zn exchange between two A-clusters, assumed to be in the most stable isomeric form in each case, due to thermodynamic control of isomer populations.

These isodesmic reactions can be modeled more accurately than most other chemical processes, since the electronic structure is qualitatively similar on both sides of the reaction equation. Specifically, we estimate the standard error for free energies *relative to a common reference cluster* to be ~10 kJ/mol. This accuracy is half of that often stated for reactions where electronic structure

changes dramatically, *e.g.* redox reactions,[54] where errors will be much larger,[40] so the error estimate is reasonable in this context.

Uncertainties due to basis set effects and surrounding chemical environment, in particular electrostatic effects, will largely cancel since they are systematic and contribute similarly on both sides of the reaction equations studied here. The electrostatic environment around any metal is very similar, and the total solvent-accessible surface is also similar in the isomeric structures, explaining the similar effect of the environment. The volumes and surfaces of computed isomers are shown in ESI, Table S10.†

All electronic structures are closed-shell d^{10}, due to the configurations of Zn^{2+} and Cd^{2+}, so a restricted computational procedure was applied. This is an additional reason for the higher accuracy than usually observed in such DFT modeling studies.

Results and discussion

1. Non-strained structures and effect of screening

In order to describe the structures of the clusters here and in future work, we introduce a measure of the non-strained (VSEPR) geometries of tetrathiolate cadmium(II) or zinc(II) complexes. Defining such geometries enables the quantification of structural distortions of individual sites. Thus, these Cd–S and Zn–S bond lengths have been computed under condense-phase electrostatic screening, modeled with BP86/Cosmo and dielectric constants of 1, 4, 6, 8, 10, 16, and 80. These numbers have been compiled in Table S1, ESI,† and are shown graphically in Fig. 3. Using these numbers as references, the inherent structural distortion caused by the A and B cluster geometries can be assessed. At the same time, they provide an estimate of the effect of screening on the geometries of the thiolate M–S bonds.

The bond lengths in Fig. 3 show that the non-strained Cd–S distance in thiolate-clusters is 2.60 Å in a homogeneous protein-like environment ($\varepsilon = 6$–10), and 2.59 Å in a highly shielded, water-like environment ($\varepsilon = 80$). The non-strained Zn–S distance is 2.39 Å ($\varepsilon = 6$–10) or 2.39 Å ($\varepsilon = 80$). Given that the uncertainty in absolute bond lengths is ~0.03 Å, the non-strained bond lengths are hardly affected by the change from 6 to 80, despite the negative charge of the clusters. This is because most of the screening effect occurs from 1 to 5, reducing all electrostatic interactions by 80%. The remaining effects are small beyond $\varepsilon = 6$, which is in the lower end of the shielding anticipated for a protein environment, 4–16.[48] *Thus, we consider 2.60 Å the equilibrium non-strained Cd–S bond length and 2.39 Å the non-strained Zn–S bond length for these tetrahedral sites and use ε = 10 in our calculations.*

The biological clusters have bridging thiolates and a total charge of −3; however the additional charge is distributed over 11 sulfur atoms and four metal ions and is also subject to screening, so the effect on each metal–sulfur bond is modest.

2. Computed geometries: accuracy and general trends

Table 1 shows the average metal–sulfur bond lengths for possible structures of the mixed Zn/Cd clusters taken from human MT-2, computed with DFT. In the bottom of Table 1, various experimental bond lengths from NMR or X-ray crystal structures are shown: these include the inorganic $[Et_4N]_2[M(S\text{-}2\text{-}Ph\text{-}C_6H_4)_4]$ complexes,[55] tetrathiophenolate $[M(tpdp)_4]^{2-}$ complexes,[56] the human Cd_7–MT-2,[27] the rat Cd_7–MT[57,58] and Zn_7–MT[58] structures, and the heterometallic rat Cd_5Zn_2–MT structure.[17] The metal sites in experimental protein structures are poorly determined, based on *a priori* fixed parameters for bonds and angles,[27,57,58] so direct comparison is made only to inorganic complexes.

As pointed out in the introduction, asymmetry of the metal sites gives rise to several isomers for each composition of cluster. Furthermore, one must distinguish two types of sulfur ligands: terminal (^{t}) and bridging (^{b}). With two metal ions available, this gives rise to four classes of bonds: Cd–S^t, Zn–S^t, Cd–S^b, and Zn–S^b. This distinction has been made before, *e.g.* in a previous DFT calculation of the Cd_4 cluster A,[37] which gave Cd–S^t = 2.54 Å and Cd–S^b = 2.59 Å, in reasonable agreement with our results for this cluster (Cd–S^t = 2.54 Å and Cd–S^b = 2.62 Å).

First, the accurate crystal data for tetrathiophenolate complexes are compared to the DFT results: the terminal Zn–S bonds are 2.33–2.35 Å, and the terminal Cd–S bonds are 2.52–2.55 Å,[55,56] in good agreement with our computed averages over all structures of 2.35 and 2.55 Å, respectively; this confirms the accuracy of the procedure.

An important observation is that terminal and bridging bonds are distinctly different: for both Zn and Cd, terminal bonds are on average 0.07 Å shorter than bridging bonds. cluster A and B give rise to similar bond lengths (± 0.02 Å) for each of these four classes of bonds, *i.e.* this electronic difference is strong enough to prevail in both cluster geometries. The average computed bond lengths for these four classes are: 2.55 Å (Cd–S^t); 2.35 Å (Zn–S^t); 2.62 Å (Cd–S^b); and 2.42 Å (Zn–S^b). The bonds in cluster B tend to be slightly longer (by 0.01–0.02 Å) than bonds in cluster A.

It is observed that the bond lengths are distributed quite accurately (± 0.05 Å) around the non-strained bond lengths computed above. This confirms that the computed non-strained bond lengths are relevant reference points for the discussion.

3. Protein structures

The experimental distances for the human Cd_7–MT-2 structure obtained from NMR[27] are given in the bottom of Table 1. The two types of Cd–S bonds are hardly distinguished in this structure: 2.61 Å (Cd–S^t), 2.59 Å (Cd–S^b) for the A-cluster, and 2.60 Å (Cd–S^t) and 2.62 Å (Cd–S^b) for the B-cluster.[27] The chosen bond length parameters do not describe the electronic terminal/bridging effect, *i.e.* all Cd–S bond lengths are similar within 0.02 Å of the non-strained Cd–S bond length. DFT can be used to improve locally these features, as is routinely done also in DFT-based refinement of crystal structures.[59]

The rat and human Cd_7–MT-2 have high sequence and secondary-structure similarity.[27,58] However, the metal site geometries differ, as reflected in the Cd–S bond lengths in Table 1. For the rat structure, the average length of all types of Cd–S bonds was set to 2.54 Å, whereas in the reported human structure, it is 2.60 Å.

The structure of rat MT-2[58] with either seven Cd^{2+} or seven Zn^{2+} bound provide a comparison of the changes accompanying the same protein under exchange from one metal to the other. Importantly, the Zn^{2+}- and Cd^{2+}-containing proteins are almost identical, in terms of 3-dimensional structure.[57] The average Cd–S bond lengths were reported as 2.54 Å, whereas the average Zn–S bond lengths were reported as 2.34 Å. No distinction between terminal and bridging bond types was again made for these structures, but the difference in average Cd–S and Zn–S bond lengths of 0.20 Å agrees very well with DFT.

Table 1 Comparison of computed and experimental average metal–sulfur bond lengths (Å)

Cluster A	Formula	Isomer	Cd–S^t_{av}	Zn–S^t_{av}	Cd–S^b_{av}	Zn–S^b_{av}	Positions[a] 380^t–381^b–382^b–379^t
Computed data, this work							
MT A calc.	Cd_4	1	2.54	—	2.62	—	Cd–Cd–Cd–Cd
MT A calc.	Cd_3Zn	1	2.54	2.35	2.62	2.43	Zn–Cd–Cd–Cd
MT A calc.		2	2.55	2.34	2.62	2.44	Cd–Cd–Cd–Zn
MT A calc.		3	2.55	2.33	2.63	2.40	Cd–Zn–Cd–Cd
MT A calc.		4	2.55	2.36	2.63	2.42	Cd–Cd–Zn–Cd
MT A calc.	Cd_2Zn_2	1	2.54	2.35	2.61	2.43	Zn–Cd–Cd–Zn
MT A calc.		2	2.55	2.35	2.62	2.41	Zn–Zn–Cd–Cd
MT A calc.		3	2.54	2.35	2.62	2.41	Zn–Cd–Zn–Cd
MT A calc.		4	2.55	2.34	2.62	2.42	Cd–Cd–Zn–Zn
MT A calc.		5	2.55	2.34	2.62	2.41	Cd–Zn–Cd–Zn
MT A calc.		6	2.55	2.34	2.64	2.40	Cd–Zn–Zn–Cd
MT A calc.	$CdZn_3$	1	2.54	2.35	2.60	2.42	Zn–Cd–Zn–Zn
MT A calc.		2	2.56	2.35	2.63	2.41	Cd–Zn–Zn–Zn
MT A calc.		3	2.54	2.35	2.60	2.42	Zn–Zn–Cd–Zn
MT A calc.		4	2.54	2.35	2.65	2.41	Zn–Zn–Zn–Cd
MT A calc.	Zn_4	1	—	2.35	—	2.41	Zn–Zn–Zn–Zn
Cluster B	Formula	Isomer	Cd–S^t_{av}	Zn–S^t_{av}	Cd–S^b_{av}	Zn–S^b_{av}	Positions[a] 378^t–377^t–376^t
MT B calc.	Cd_3	1	2.56	—	2.63	—	Cd–Cd–Cd
MT B calc.	Cd_2Zn	1	2.56	2.35	2.63	2.43	Cd–Cd–Zn
MT B calc.		2	2.56	2.36	2.63	2.42	Cd–Zn–Cd
MT B calc.		3	2.56	2.35	2.63	2.43	Zn–Cd–Cd
MT B calc.	$CdZn_2$	1	2.56	2.36	2.63	2.42	Zn–Zn–Cd
MT B calc.		2	2.57	2.35	2.62	2.43	Zn–Cd–Zn
MT B calc.		3	2.56	2.36	2.62	2.42	Cd–Zn–Zn
MT B calc.	Zn_3	1	—	2.36	—	2.42	Zn–Zn–Zn
AVERAGE			2.55	2.35	2.62	2.42	
Experimental data, previous work							Notes
$[Et_4N]_2[M(S\text{-}2\text{-}Ph\text{-}C_6H_4)_4]$		Ref. 55	2.52	2.34	—	—	
$[M(tdpd)_2(N\text{-}MeIm)_2]$		Ref. 56	2.52–2.55	2.33–2.35			
Human Cd_7–MT2	Cd_4	Ref. 27	2.61	—	2.59	—	1MHU.pdb A-cluster
Human Cd_7–MT2	Cd_3	Ref. 27	2.60	—	2.62	—	2MHU.pdb B-cluster
Rat Cd_7–MT2	Cd_4+Cd_3	Ref. 58	2.54 ± 0.02 avr. Cd–S	—	A+B clusters		
Rat Zn_7–MT2	Zn_4+Zn_3	Ref. 58	—	2.34 ± 0.03 avr. Zn–S	A+B clusters		
Rat Cd_5Zn_2–MT	Cd_4	Ref. 17	2.50	—	2.52	—	A cluster
Rat Cd_5Zn_2–MT	$CdZn_2$	Ref. 17	2.49	2.36	2.54	2.40	B cluster
Computational data, previous work							
Human MT2	Cd_4	Ref. 37	2.54	—	2.59	—	Cluster A, DFT (P86)

[a] The t and b refers to metal sites being in "terminal" and "bridging" positions, *i.e.* having two or one terminal cysteines bound, respectively. In the B cluster, all metal ions bind two bridging and two terminal sulfur atoms and are designated "t".

Structures have also been obtained for the heterocluster B $[Cd_2ZnCys_9]^{3-}$ and homocluster A $[Cd_4Cys_{11}]^{3-}$ in heterometallic Cd_5Zn_2–MT rat protein (4MT2.pdb).[26] The experimental observation of a heterocluster is interesting in itself, and may indicate how the introduction of Cd^{2+} affects the remaining zinc ions in a protein, although direct comparison to human MT-2 is not straight-forward. In this structure, terminal and bridging cysteines have been distinguished: the Zn–S^t bond lengths are 2.36 Å on average, and the Zn–S^b bonds are 2.40 Å on average, very similar to within 0.01–0.02 Å of DFT. Both the Zn^{2+} ions are situated in the B-cluster. On the other hand, the Cd–S^t bond lengths are 2.50 Å on average in the A-cluster and 2.49 Å on average for the single Cd^{2+} in the B-cluster. The Cd–S^b bond lengths are 2.52 Å for the A-cluster and 2.54 Å for the B-cluster.[26]

The trend of longer bridging bonds of 0.02–0.05 Å is in some accordance with DFT, which gives ~0.07 Å longer bridging bonds. The difference between Cd–S and Zn–S bonds, which was 0.20 Å from DFT and other rat structures, has been reduced to 0.14–0.15 Å in the heterometallic rat structure.

In general, the use of *ad hoc* parameters for metal–ligand bonds in the refinement of metalloprotein structures means that the geometries of metal sites are not very accurately described experimentally for normal-size proteins.[59] The structures of MTs thus reflect the choices of parameters for Cd–S and Zn–S bonds and the constraints towards tetrahedral coordination geometry imposed during refinement, and the present DFT data can serve as a relevant complement to these structures, perhaps also for future refinement of protein structures.

4. Structural characterization of computed isomers

The first part of Table 1 shows the average, computed metal–sulfur bond lengths for all isomers possible from each composition of

Table 2 Average bond orders for types of bonds, obtained from Mulliken population analysis, averaged over all isomers

	Cluster A					Cluster B			
	M380	M381	M382	M379	*Average*	M378	M377	M376	*Average*
Cd–S^b	0.59	0.64	0.64	0.57	0.61	0.62	0.64	0.59	0.61
Cd–S^t	0.84	0.89	0.88	0.87	0.87	0.83	0.81	0.88	0.84
Zn–S^b	0.79	0.83	0.83	0.77	0.80	0.81	0.81	0.79	0.80
Zn–S^t	0.97	0.98	0.97	0.99	0.98	0.96	0.94	0.98	0.96

Table 3 Average atomic charges derived from Mulliken population analysis (in atomic units)

	Cluster A	Cluster B
S^t (Cd)	–0.45	–0.47
S^t (Zn)	–0.45	–0.47
S^b	–0.28	–0.28
Cd	0.41	0.44
Zn	0.45	0.43

cluster. The structures and anticipated stabilities of each isomer will be unique and depend on the position of the Cd^{2+} *vs.* Zn^{2+} in each of the four or three sites in the clusters. Another observation is that the bond length of each type of bond is relatively insensitive to the overall isomeric form and composition of the cluster, with maximum differences of +/− 0.03 from the average 2.55 Å (Cd–S^t), 2.35 Å (Zn–S^t), 2.62 Å (Cd–S^b), and 2.42 Å (Zn–S^b).

There are two simple ways to measure the structural strain in tetrahedral sites: bond distortions (compression or elongation) of metal–ligand bonds, and angular distortions away from the VSEPR-optimal, 109.5°. The deviation from non-strained bond lengths have been compiled for each type of bond in each isomer (data are available in ESI, Table S11†). The terminal bonds are generally compressed compared to the non-strained bond length, on average by 0.05 Å for Cd and 0.04 Å for Zn, whereas the bridging bonds are generally elongated compared to non-strained, by 0.02 Å on average for Cd and 0.03 Å for Zn. Individual variations are small.

The results of Mulliken population analysis have been included in Tables S12 and S13, ESI,† and the most relevant average bond orders and atomic charges are shown in Tables 2 and 3. In general, Mulliken population analysis works best for trend descriptions, as the absolute numbers are highly sensitive to basis set effects. The bond orders in Table 2 are as expected anticorrelated with the M–S bond lengths. The average bond orders for Cd–S^b, Cd–S^t, Zn–S^b, and Zn–S^t, are 0.61, 0.87, 0.80, and 0.98, respectively in cluster A, and very similar within 0.03 in cluster B. Thus, the terminal M–S bond orders are close to 1, whereas the bridging bonds are substantially weaker. Also, the Zn–S bonds generally exhibit higher bond orders by 0.10–0.20.

The weaker bridging bonds and the stronger terminal bonds can be explained from electrostatic considerations: first, the relaxed BP86/DZP bond dissociation curves of bonds M1–S2 and M1–S4 in Cd_3 and Zn_3 clusters are given in Fig. S1, ESI,† and provide a quantitative estimate of the bond strengths, *ca.* 50, 42, 37, and 33 kJ/mol for Zn–S^t, Cd–S^t, Zn–S^b, and Cd–S^b, fully consistent with bond orders and bond lengths. Second, from Table 3, the average atomic charges of the terminal sulfur atoms are –0.45/–0.47 a.u. in cluster A/B, whereas the bridging sulfur atoms share their negative charge between to metal centers and are 0.17–0.19 a.u. less negative. Thus, smaller polarization correlates with weaker bonds. This effect will exist also in the proteins, possibly partially counteracted by the protein scaffold. It will cause the sites to exhibit varying selectivity and thus, the observation is of biological relevance.

The S–M–S angles provide another quantification of structural distortion away from tetrahedral. In Fig. 4, the squared angular deviations of all S–M–S angles from 109.5°, summed over all sites in the cluster, have been compiled for each cluster. There are six such angles for each metal site. It can be seen that the average squared angular distortion of a cluster is 300 squared degrees, corresponding to about 75–100 squared degrees for an individual site. Variations between isomers are up to ±200 squared degrees. Thus, unlike the bond lengths, which have large force constants associated with them, the S–M–S angles deviate substantially for different isomers.

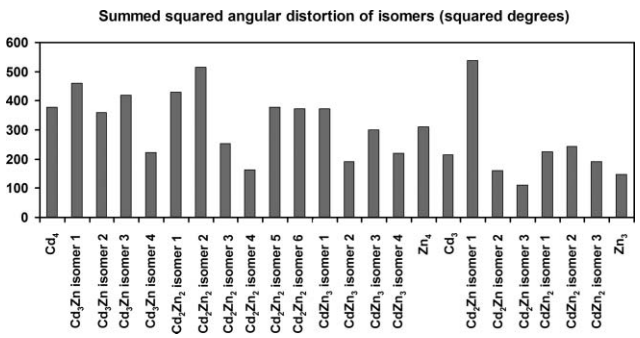

Fig. 4 Summed squared angular deviations from 109.5° of all S–M–S angles, measured in squared degrees, computed for each isomer.

We now investigate whether there are any trends in the extent of distortion for each type of site. For this purpose, we distinguish all seven sites (379, 380, 381, and 382 in cluster A and 376, 377, and 378 in cluster B) as well as whether Zn^{2+} or Cd^{2+} is bound in the site. This gives a total of 14 characteristic metal sites.

Fig. 5 shows how the distortion is distributed on these 14 types of sites. The general cluster architecture remains intact for all isomers, with all metal ions pseudo-tetrahedrally coordinated. The extent of distortion differs substantially: the B-cluster sites 376 and 377 are among the least distorted, together with site 380 of cluster A. However, site 378 in cluster B is on the other hand the most distorted. Thus, the sites in cluster B differ widely in extent of distortion, whereas in cluster A, the distortion is more equally distributed among the four sites.

It can also be calculated from the data in Fig. 5 that on average, sites are less angularly distorted when occupied by Zn^{2+} (74 degrees squared) than by Cd^{2+} (90 degrees squared). This implies that,

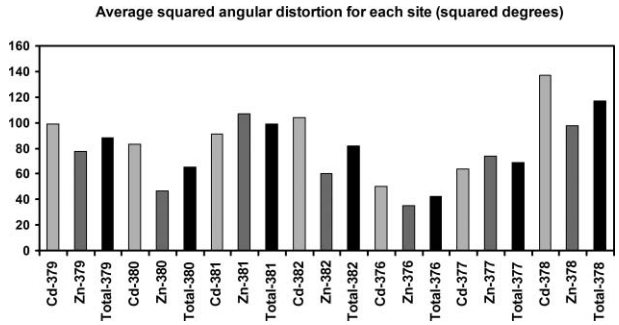

Fig. 5 Average squared angular deviations (squared degrees) of all S–M–S angles from 109.5°, computed for each type of metal site: 7 distinct sites, 14 if distinguishing Cd^{2+} and Zn^{2+}.

averaged over all possible isomers, the architecture is closer to T_d symmetry for Zn^{2+}, whereas Cd^{2+} imposes more asymmetry.

In the B cluster, all metal ions bind two bridging and two terminal sulfur atoms and are designated "t".

In conclusion, the structural analysis of all possible isomers of cluster A and B with Zn^{2+} and Cd^{2+} reveals minor variations (+/− 0.02 Å) in bond lengths within the four classes of bonds, with averages of 2.55 Å (Cd–S^t); 2.35 Å (Zn–S^t); 2.62 Å (Cd–S^b); and 2.42 Å (Zn–S^b). However, each site is unique due to the asymmetry of the cluster architectures, and this causes the angular distortions to differ widely, both between isomers averaged over all sites and between individual sites averaged over all isomers.

5. Stabilities of isomers: free energy computations

The observed intrinsic asymmetry of the clusters will cause them to exhibit varying metal ion selectivity, and hence, isomers will not have the same stability in the MT clusters and will thus not occur in the statistically average compositions observed for simple inorganic clusters. This observation has biological implications for the selectivity and composition of the clusters and hence, we will attempt to describe this relative stability of isomers in the following. Table 4 shows the computed relative electronic energies (ΔE_{el}), enthalpies (ΔH), entropies ($T\Delta S$), and Gibbs free energies (ΔG) of the various possible isomers for each composition in the two cluster types. All state functions were computed relative to the isomer with the smallest free energy and should be viewed in this relative context. By comparing the relative free energies, the most stable isomer can be identified for each stoichiometry.

The overall stability depends on the subtle compensation of both enthalpic and entropic effects. In the isomers where enthalpy and entropy contributions are of the same sign, the state functions compensate. This common situation occurs in all but four cases, including all isomers of cluster B. Interestingly, in four cases – all found in cluster A – both entropy and enthalpy are unfavorable to an isomer relative to the most stable isomer.

Except for three cases (−12.4 kJ/mol, −11.8 kJ/mol, and +13.4 kJ/mol) all entropic effects are within +/− 10 kJ/mol. However, some isomers are particular unstable in terms of free energy, namely four isomers of cluster A; isomer 1 of Cd_3Zn and isomer 1–3 of Cd_2Zn_2; and two isomers of cluster B; isomer 3 of Cd_2Zn and isomer 1 of $CdZn_2$. In all these cases, enthalpy is the main reason for the instability, implying the involvement

Table 4 Relative electronic energies and free energies of computed isomers (kJ/mol)

Cluster A	Isomer	ΔE_{el}	ΔH	$T\Delta S$	ΔG	Positions[a] 380^t–381^b–382^b–379^t
Cd_3Zn	1	42.4	39.0	−5.9	44.9	Zn–Cd–Cd–Cd
	2	0.3	2.7	2.5	0.2	Cd–Cd–Cd–Zn
	3	0.0	0.0	0.0	0.0	Cd–Zn–Cd–Cd
	4	3.5	3.3	0.6	2.6	Cd–Cd–Zn–Cd
Cd_2Zn_2	1	35.0	31.4	−6.7	38.0	Zn–Cd–Cd–Zn
	2	35.5	37.4	9.6	27.7	Zn–Zn–Cd–Cd
	3	34.1	35.9	6.9	28.9	Zn–Cd–Zn–Cd
	4	7.2	6.9	−4.1	11.0	Cd–Cd–Zn–Zn
	5	0.0	0.0	0.0	0.0	Cd–Zn–Cd–Zn
	6	7.4	4.2	−2.9	7.1	Cd–Zn–Zn–Cd
$CdZn_3$	1	10.1	8.9	7.7	1.1	Zn–Cd–Zn–Zn
	2	−1.7	−5.0	−7.2	2.2	Cd–Zn–Zn–Zn
	3	3.5	−1.5	−12.4	10.9	Zn–Zn–Cd–Zn
	4	0.0	0.0	0.0	0.0	Zn–Zn–Zn–Cd

Cluster B	Isomer	ΔE_{el}	ΔH	$T\Delta S$	ΔG	Positions[a] 378^t–377^t–376^t
Cd_2Zn	1	0.0	0.0	0.0	0.0	Cd–Cd–Zn
	2	0.0	−2.4	−11.8	9.5	Cd–Zn–Cd
	3	22.9	25.8	8.0	17.8	Zn–Cd–Cd
$CdZn_2$	1	15.6	18.8	1.5	17.3	Zn–Zn–Cd
	2	17.4	20.1	13.4	6.8	Zn–Cd–Zn
	3	0.0	0.0	0.0	0.0	Cd–Zn–Zn

[a] The t and b refers to metal sites being in "terminal" and "bridging" positions, *i.e.* having two or one terminal cysteines bound, respectively. In the B cluster, all metal ions bind two bridging and two terminal sulfur atoms and are designated "t".

of differential electronic and/or electrostatic effects in the bonds rather than differing flexibilities of the isomeric structures.

From Table 4, it can further be observed that some sites tend to have a preference for Zn^{2+} and others for Cd^{2+}. In fact, all the six least stable isomers have Zn^{2+} in site 380 in cluster A and 378 in cluster B, and an estimate shows that the penalty paid for this is ~35 kJ/mol in cluster A. Thus, the computations of the various isomers converge on the view of this site as especially selective towards Cd^{2+}. This does not mean that it has the highest affinity for Cd^{2+}, but the highest *relative affinity* (selectivity) for Cd^{2+} as compared to Zn^{2+}. The observation of substantial metal ion selectivity already at the intrinsic cluster level was anticipated from the observation of seven structurally distinct asymmetric sites.

When only one Cd^{2+} resides in cluster A, it is least favorable to have it in site 382 by ~10 kJ/mol, *i.e.* Cd^{2+} can sit virtually anywhere. This $CdZn_3$ stoichiometry is neutral with respect to the position of Zn^{2+} in site 380, suggesting that the unfavorable arrangement of Zn^{2+} in site 380 only occurs with exposure to more than one Cd^{2+} ion. The reason is most likely the larger distortion caused with more Cd^{2+}, which stresses site 380 and reduces the affinity for Zn^{2+}. Once the first Cd^{2+} has distorted the cluster, other sites are more susceptible to binding Cd^{2+}, relative to Zn^{2+}.

In cluster B, occupation of sites 376 and 378 determine stability: If 376 is occupied by Cd^{2+}, free energy increases by ~10 kJ/mol, compared to Zn^{2+}. If site 378 is occupied by Zn^{2+} instead of Cd^{2+}, the free energy increases by approximately 7 kJ/mol. This is also the most angularly distorted site in general, implying selectivity in favor of Cd^{2+}. Site 377 is neutral with respect to occupancy. The

two effects are cumulative and thus, the least stable isomers of each heterocluster both have Cd^{2+} in site 376 and Zn^{2+} in site 378 and free energies of ~17–18 kJ/mol.

The relative stabilities in Table 4 indicate that several of the isomers are in thermodynamic equilibrium at room temperature. Since the standard error is estimated to be ~10 kJ/mol, we use a cutoff of 10 kJ/mol to rule out thermodynamically inaccessible isomers. This criterion leaves three isomers (2–4) for Cd_3Zn, two isomers (5–6) for Cd_2Zn_2, 3 isomers (1,2 and 4) for $CdZn_3$, 2 isomers (1 and 2) for Cd_2Zn, and two isomers (2 and 3) for $CdZn_2$.

The comparison of free energies of isomers to their corresponding angular distortions shows that there is no significant correlation between total angular distortion and stability. Instead, the stability is related to the position of metal ions within specific sites, with site 380 in cluster A and site 378 in cluster B both having a strong preference for Cd^{2+}. In cluster B, site 376 has an equally strong preference for Zn^{2+}.

6. Compositions of cluster A + B together in equilibrium

Even though clusters A and B can not be compared directly in terms of free energy due to their different chemical composition, the preference of metal ions for each cluster can be computed once the most stable isomers have been identified. This is achieved by calculating the free energies of hypothetical metal exchange reactions as the one occurring in eqn (3), which describes exchange between A and B clusters:

$$[Cd_mZn_{4-m}(SCH_3)_{11}]^{3-} + [Cd_nZn_{3-n}(SCH_3)_{11}]^{3-} \rightarrow [Cd_{m+1}Zn_{3-m}(SCH_3)_{11}]_L^{3-} + [Cd_{n-1}Zn_{4-n}(SCH_3)_{11}]^{3-} \quad (3)$$

Table 5 shows the enthalpies, entropies, and free energies calculated for each possible metal exchange between cluster A and cluster B, using the most stable isomers for the computation. Given that the composition of the clusters is thermodynamically controlled,[28] the free energy of these reactions will pinpoint the most stable occupancy between the two clusters in at any Cd^{2+}-load.

At low Cd^{2+}-load (maximum 1 Cd^{2+} per A and B cluster), the main question is whether the Cd^{2+} ion will be accommodated into the A-cluster or B-cluster. The free energy of exchanging Cd^{2+} and Zn^{2+} from cluster A to B (computed from most stable isomers) is –27 kJ/mol in favor of having Cd^{2+} situated in the B-cluster. Thus, the computations predict the first Cd^{2+} to enter into the B-cluster, at site 377 or 378. These two sites have the highest selectivity for Cd^{2+} and are also the most angularly distorted sites of cluster B, in good line with larger angular distortion facilitating Cd^{2+} coordination.

When the Cd^{2+}-concentration increases, some clusters may contain two Cd^{2+} ions. There are three general ways of distributing two Cd^{2+} ions among an A-cluster and a B-cluster, namely both situated in cluster A, both in cluster B, or one in each cluster. In good accordance with the results for only one Cd^{2+} ion, having two Cd^{2+} ions in cluster A is slightly less favorable (by 3 kJ/mol) than having one in each cluster, whereas having both Cd^{2+} ions in cluster B is 12 kJ/mol more stable than having one Cd^{2+} in each cluster. While the first result is not very significant due to the computational uncertainty, the results imply that both Cd^{2+} ions will be situated in cluster B, most likely in site 377 and 378, when the protein scaffold is absent.

Table 5 Enthalpies, entropies, and free energies of metal exchange from A to B clusters' most stable isomers (kJ/mol)

ΔH	$T\Delta S$	ΔG	Metal exchange reaction[a]
1 Cd + 6 Zn			
0.2	27.7	–27.4	$CdZn_3 + Zn_3 =$ **$CdZn_2 + Zn_4$**
2 Cd + 5 Zn			
11.9	14.6	–2.7	$Cd_2Zn_2 + Zn_3 = CdZn_3 + CdZn_2$
–1.4	10.9	–12.3	$CdZn_3 + CdZn_2 =$ **$Zn_4 + Cd_2Zn$**
3 Cd + 4 Zn			
–5.7	12.3	–18.0	$Cd_3Zn + Zn_3 =$ **$Cd_2Zn_2 + CdZn_2$**
15.3	5.0	10.2	$Cd_2Zn_2 + CdZn_2 = CdZn_3 + Cd_2Zn$
36.3	5.8	30.5	$CdZn_3 + Cd_2Zn = Zn_4 + Cd_3$
4 Cd + 3 Zn			
–54.1	12.8	–66.9	$Cd_4 + Zn_3 = Cd_3Zn + CdZn_2$
–2.3	2.8	–5.1	$Cd_3Zn + CdZn_2 =$ **$Cd_2Zn_2 + Cd_2Zn$**
53.0	–0.1	53.1	$Cd_2Zn_2 + Cd_2Zn = CdZn_3 + Cd_3$
5 Cd + 2 Zn			
–50.7	3.2	–53.9	$Cd_4 + CdZn_2 =$ **$Cd_3Zn + Cd_2Zn$**
35.4	–2.3	37.7	$Cd_3Zn + Cd_2Zn = Cd_2Zn_2 + Cd_3$
6 Cd + 1 Zn			
–13.0	–1.9	–11.1	$Cd_4 + Cd_2Zn =$ **$Cd_3Zn + Cd_3$**

[a] Bold shows most stable composition.

With a 3 : 4 : 1 : 1 molar ratio for $Cd^{2+} : Zn^{2+} : A : B$, there are four possible compositions: all three Cd^{2+} ions in cluster A, two in cluster A and one in cluster B, one in cluster A and two in cluster B, or all three in cluster B. From Table 5, it can be seen that having all three in cluster A is unfavorable by 18 kJ/mol compared to having one Cd^{2+} in cluster B. This composition is more favorable by 10 kJ/mol than having two Cd^{2+} in cluster B, which is much more favorable by 53 kJ/mol than having all three Cd^{2+} in cluster B, forming two homoclusters. Thus, the calculations point towards the heteroclusters being preferred at this Cd^{2+} load, in particular, the $Cd_2Zn_2 + CdZn_2$ composition. This favorable composition consists of a mixture of isomers, with isomers 5 + 3, 5 + 2, 6 + 3 being most stable.

Next, the situation where the molar ratio is 4 : 3 : 1 : 1 for $Cd^{2+} : Zn^{2+} : A : B$ is considered, giving four possibilities. From the computed free energies in Table 5 it can be seen that the homo cluster distribution is again highly unfavorable, by 67 kJ/mol compared to $Cd_3Zn + CdZn_2$. This composition and the $Cd_2Zn_2 + Cd_2Zn$ composition are however equally stable, with a small (5 kJ/mol) preference for the latter. The configuration where one homocluster is present instead of two, $CdZn_3 + Cd_3$, is unfavorable by 53 kJ/mol compared to $Cd_2Zn_2 + Cd_2Zn$. Thus, the four Cd^{2+} ions are distributed with two in each cluster, or alternatively three in cluster A.

For the $Cd_2Zn_2 + Cd_2Zn$ composition, three isomers are in thermodynamic equilibrium within 10 kJ/mol; 5 + 1, 6 + 1, and 5 + 2. For the $Cd_3Zn + CdZn_2$ composition, six isomeric forms may be in equilibrium, namely 2 + 2, 2 + 3, 3 + 2, 3 + 3, 4 + 2, and 4 + 3.

When Cd^{2+} load dominates in a 5 : 2 : 1 : 1 ratio for $Cd^{2+} : Zn^{2+} : A : B$, there are three options possible for overall cluster composition: two Zn^{2+} in cluster A, two in each cluster, or two in cluster B. Again, having a homocluster is quite unfavorable

(by 38 or 54 kJ/mol) compared to having two heteroclusters. Thus, the $Cd_3Zn + Cd_2Zn$ composition is observed, most likely consisting of a number of isomers, *i.e.* 2 + 1, 2 + 2, 3 + 1, 3 + 2, and 4 + 1 with free energies within 10 kJ/mol. In all these, Cd^{2+} will have taken up position 380 in cluster A and position 378 in cluster B.

The last situation investigated has only one Zn^{2+} ion per 6 Cd^{2+} ions. Under such conditions, it is 11 kJ/mol more favorable to have the Zn^{2+} ion situated in cluster A. Three isomers of Cd_3Zn, 2, 3, and 4, are expected to be in thermodynamic equilibrium.

In summary, at low cluster concentration, usually one or two compositions are possible for a given Cd^{2+} load, and within these compositions, we have identified a number of isomers that are likely to exist in equilibrium. This can be related to NMR data for the rabbit Cd_4Zn_3–MT, which revealed a non-uniform distribution of both metals,[68] and electrochemical studies that revealed several forms of human MT in solution depending on Cd^{2+} and Zn^{2+} concentration.[22]

At moderate Cd^{2+} load, the calculations reveal a mixture of many isomers. The proteins may affect the relative stability of isomers, mainly spatial constraints from the backbone. However, the thermodynamically governed favoritism of heteroclusters at high Cd^{2+} concentration is in accordance with observations from Cd^{2+}/Zn^{2+} exchange between Zn_7–MT and Cd_7–MTs:[35] at 2 : 1 $Cd^{2+} : Zn^{2+}$ concentration, $Cd_2Zn_2 + Cd_3Zn$ and $Cd_2Zn + CdZn_2$ compositions were observed for A and B clusters, respectively.[35] We found that at 4Cd + 3Zn stoichiometry, $Cd_2Zn_2 + Cd_2Zn$ dominates, however with only 5 kJ/mol to $Cd_3Zn + CdZn_2$ (Table 5), with no homoclusters present. At 5Cd + 2Zn stoichiometry, we found $Cd_3Zn + Cd_2Zn$ to be the only species.

Hence, the experimental observations by Otvos *et al.* of distinct heteroclusters at these Cd^{2+} loads are readily explained from intrinsic properties of the A and B clusters, without protein scaffold present. Given the small size of metalloproteins, this may have been anticipated, as a small protein cannot enforce large electrostatic or steric constraints on these clusters, which make up a substantial fraction of total molecular mass.

7. Compositions at high cluster concentration

So far, we have discussed the cluster concentration as being infinitely low, with one of each cluster exposed to an increasing number of Cd^{2+} ions. The data in Table 5 imply that at low Cd^{2+} load, the Cd^{2+} will enter the more angularly distorted site 378 (or possibly 377) of cluster B. However, when more clusters are available to accommodate the Cd^{2+} and Zn^{2+} ions, the situation becomes slightly more complicated. Now, in principle several Cd^{2+} ions could go into two different cluster Bs and leave cluster As intact. From the free energies of metal transfer between two clusters of the same type (A or B), it can be deduced whether any special effects are encountered when more clusters of each type are available for the Cd^{2+} ions.

Table 6 shows the reaction free energies for exchange between two sets of clusters when the Cd^{2+} and cluster concentrations are comparable (2 : 2 : 2 for $Cd^{2+} : A : B$). This situation gives rise to five different states: one Cd^{2+} in each cluster A; one in a cluster A and one in a cluster B; one in each cluster B; two in one cluster A; or two in one cluster B.

Table 6 Enthalpies, entropies, and free energies of metal exchange between two sets of clusters with two Cd^{2+} ions available (kJ/mol)

ΔH	$T\Delta S$	ΔG	Metal exchange reaction
0.2	27.7	−27.4	$CdZn_3 + CdZn_3 + Zn_3 + Zn_3 = CdZn_3 + Zn_4 + CdZn_2 + Zn_3$
−9.5	40.9	−50.4	$CdZn_3 + CdZn_3 + Zn_3 + Zn_3 = Zn_4 + Zn_4 + CdZn_2 + CdZn_2$
−16.6	5.9	−22.5	$CdZn_3 + CdZn_3 + Zn_3 + Zn_3 = Cd_2Zn_2 + Zn_4 + Zn_3 + Zn_3$
−6.1	31.4	−37.5	$CdZn_3 + CdZn_3 + Zn_3 + Zn_3 = Zn_4 + Zn_4 + Cd_2Zn + Zn_3$

The computed reaction free energies in Table 6 all start from the least favorable composition of having two homo-B-clusters and one Cd^{2+} in each cluster A. It is most favorable to distribute one Cd^{2+} ions in each B-cluster, 50.4 kJ/mol more favorable than the least stable state. The second-most stable state is having both Cd^{2+} ions in one of the B-clusters, 13 kJ/mol less favorable than the ground state (−37.5 kJ/mol more stable than the least stable state). Thus, it can be deduced that at comparable cluster and Cd^{2+} concentrations, the Cd^{2+} ions will occupy as many B-clusters as possible, before occupying A-clusters.

8. Biological implications

Zn^{2+} homeostasis is now beginning to be fully appreciated, perhaps in particular in the brain:[16] Zn^{2+} has been found to modulate synaptic plasticity as a co-transmitter;[16] Zn^{2+} is involved in inflammation and anti-oxidative response *via* a variety of enzymes, *e.g.* superoxide dismutase, in Zn^{2+}-dependent inhibitory sites,[10] and in the regulation of many proteins by Zinc-finger dependent transcription factors. It has been shown that MTs transfer Zn^{2+} to several, possibly all, of the targets mentioned above.[10,60,61] MTs serve multiple other roles, including both heavy metal detoxification, Zn^{2+} ion homeostasis, and possibly oxidative stress control.[62] Given the importance of MTs, structure-function correlations of the involved metal-binding clusters is a natural step forward.

Most of the Cd^{2+} that organisms are exposed to is bound to MTs.[24,25] The concentration of Cd^{2+} (as well as other heavy metals) rise with age, more so for smokers and old females;[63,64] Cd^{2+} has a physiological half-life of 10–30 years.[65] Since Cd^{2+} binds more strongly to human MTs than Zn^{2+}, Zn^{2+} is released in this process:[31,67] Electrochemical studies have shown that in human MTs, Cd^{2+} substitutes Zn^{2+}, releases free Zn^{2+}, and gives rise to several complexes that are hard to distinguish in NMR spectra.[22] It has been shown that Cd^{2+} substitutes Zn^{2+} isomorphously, retaining the general structure,[26,66,67] confirming that the overall folds of MTs are robust and similar once metal ions are bound. Evidence of several forms of heteroclusters of Cd_4Zn_3–MT stoichiometry has been obtained from ^{113}Cd NMR studies.[68] This suggests that the heteroclusters in MTs consist of more isomers in thermodynamic equilibrium. NMR studies found that the Zn^{2+} ions in the B cluster are more labile than those in the A cluster under exposure to nitric oxide.[69]

Whether the Zn_6–MT form of MT-2 has life time enough to exist *in vivo*,[4] so that Cd^{2+} binding occurs to this species (dissociative

substitution), or whether Cd^{2+} binding occurs by associative or concerted substitution into Zn_7–MT2, which in some reports has a stability constant of 3×10^{13} M^{-1}, is a matter of debate, and there is also substantial debate about the co-operative nature of these substitutions.[29] However, since the kinetic lability of metal ions in MTs is generally high,[28] the actual composition of MTs will be subject to thermodynamic control, in accordance with the homeostatic regulation roles that these proteins have. Thus, to understand at a molecular level the function and dysfunction of MTs one must examine the thermodynamically stable isomers shown in this work to arise upon chemical modification, in the present case exposure to Cd^{2+}.

The effects of heavy metal ions in compromising the vital functions of MTs are currently not understood. Insight into the observed[24,25] Cd^{2+} binding to MTs is thus important, both to understand the mechanism of detoxification by MTs, and to understand how chemical modifications may affect MT function in relation to Zn^{2+} homeostasis, including release of free Zn^{2+}.[5,9,10,11,12,13] We have seen that the MT clusters are intrinsically highly asymmetric.

In the case of small inorganic metal thiolate models, mixing of two homoclusters always gives rise to heteroclusters of nearly statistical distribution.[70] In the A and B clusters, such a simple distribution is not obtained due to the asymmetry imposed by the cluster architecture itself. This asymmetry is part of the reason for the experimentally observed differences in metal affinities of each site.[31,32] Two types of asymmetry have previously been hypothesized to serve important roles in the structure–function correlations of MTs: one is structural distortion due to cluster architecture, which can be described mainly *via* the deviation of S–M–S angles from tetrahedral, 109.5°.[20] The other is the distinction between bridging and terminal cysteines, which necessarily must cause differences in the A-cluster.[5] The effect of distortions accompanying chemical modifications may lead to an understanding of MT dysfunction.

It was found here that Cd^{2+}/Zn^{2+} selectivities correlate with angular distortion of the sites: the more distorted sites favor Cd^{2+} over less distorted sites, relative to Zn^{2+}. The selectivities are modeled with an estimated accuracy of ~10 kJ/mol. We have identified one site in cluster A, 380, which particularly prefers Cd^{2+}, with other sites being more or less neutral to Zn^{2+}/Cd^{2+} differentiation. In cluster B, we have identified site 378 as having larger selectivity for Cd^{2+}, and 376 as having a larger selectivity for Zn^{2+}. These preferences are consistent among the various isomers and may imply a special functional role of these sites.

We have identified the isomers that, assuming thermodynamic control, will be relevant *in vivo* if the protein would not provide any contribution to selectivity, which it clearly will. Table 5 shows which compositions are most stable at various Cd^{2+} loads (in bold) and Table 4 shows which isomers are most stable for each composition. At 2 : 1 Cd^{2+} : Zn^{2+} stoichiometry, the DFT calculations can explain the experimental observations of heteroclusters upon mixing Cd_7–MT and Zn_7–MT.[35] As discussed in that work, equlibration of stoichiometry between individual MTs occurs, and *in vivo* expression of MT-2 may be exactly such as to ensure these compositions prevail, *i.e.* higher or lower Cd^{2+} loads are unwanted.

The preference for heteroclusters would be entropically driven in a purely symmetric system with statistical distribution occurring. However, as seen in Table 5, the preference for heteroclusters is enthalpically controlled, which means it must be understood from electronic interactions. The preference for heteroclusters is reflected in the free energies of Table 4: there are sites in both clusters with strong selectivity towards Cd^{2+} over Zn^{2+} and *vice versa*.

The MT clusters have unusually large charge densities as reflected in their formal –3 charges. This is particularly true for the smaller B-cluster having molecular volumes of ~ 4169–4416 $Å^3$, about 20% smaller than the A clusters (see Table S10, ESI†). Since Zn brings negative charges closer in space due to the ~0.2 Å M–S bond lengths (see Table 1), and since the atomic charges of terminal sulfur atoms, metal ions, and bridging sulfur atoms, respectively, do not change much from Zn^{2+} to Cd^{2+} and cluster type (Table 3), the Zn ions will be distributed in both clusters at moderate Cd load to minimize charge repulsion. This simple principle can explain why heteroclusters are enthalpically favored, a question raised by Otvos and co-workers but not answered.[35]

The knowledge gained here shows that the preferences for heteroclusters occur already at the intrinsic cluster levels, without the presence of protein. The protein is not expected to affect this preference by electrostatics since charge distributions are very similar in the various isomers; however it could do so *via* steric strain of the backbone on various individual sites enforcing some spatial selectivity. This second option is not necessary to explain the existence of heteroclusters but may be necessary to explain quantitatively the affinities and selectivities of each site. This will be studied in a subsequent work where various protein scaffolds are included in the calculations.

We have examined the intrinsic properties of inorganic A- and B-clusters, and found that they are clearly distinct, asymmetric structures with four, respectively three unique sites. The evolutionary benefit of having two clusters (A and B) can be hypothesized upon. The tendency of any Cd^{2+} to enter first into cluster B, both at 1 : 1 and 1 : 2 molar ratios of protein : Cd^{2+} could imply that cluster B may contain most of the heavy metal ions at low Cd^{2+} exposure, possibly allowing cluster A to maintain function even at a this Cd^{2+} concentration. This is in good agreement with results obtained by Li and Otvos using Ag^+ and Cu^+ ions.[71] A possible advantage of this, suggested by these authors, could be that the MT is functional even after metal detoxification, *i.e.* when heavy metal ions are bound to cluster B, cluster A remains intact and can function in Zn^{2+} transfer. Had the Cd^{2+} entered randomly with the same statistical weight into both clusters, all sites would be affected by the Cd^{2+} binding. We have clearly seen that this is not the case: heteroclusters form, but substantial selectivity occurs between sites within each cluster. Our results show that this ability can be explained already due to the inherent properties of the cluster A and B structures.

The protein scaffold may affect selectivity within the individual subunits due to spatial constraints.[68] The larger average volume per site will favor Cd^{2+}. While this protein effect will need to be quantified, it is clear from this work that it is not large enough to counteract the intrinsic preference for heteroclusters at biologically relevant moderate Cd^{2+} load, *i.e.* there is not a large enough difference in average available volumes in MT subunits to force homoclusters to form. The COSMO-computed solvent accessible volumes of individual clusters (Table S10, ESI†) show that indeed, Cd^{2+} takes up more volume, but there are smaller individual variations among isomers of the same stoichiometry.

The small size of MTs may be a main reason why the intrinsic preferences found in the clusters prevail also in proteins: the main function of the protein scaffold may then be to simply stabilize the metal clusters, as these clusters have evolved to inherently contain most of the biologically relevant metal ion selectivity.

Understanding the many available states of these proteins may elucidate how Zn^{2+} and possibly other metal ions can be transferred from MT to other proteins, and how heavy metal exposure, pH or oxidative stress may disrupt this transfer. Apparently, only the most labile Zn^{2+} is transferred, and the composition of the MT at that time is thermodynamically controlled.[72,73] Dysfunction of MTs due to the above-mentioned effects may have severe consequences in handling oxidative stress and in *e.g.* neurological disorders.[7,16] Thus, this work's identification of intrinsic asymmetric cluster architectures and associated selectivities and the identification of various stable isomeric forms will be followed by further work in these other directions.

Conclusions

This paper has reported electronic–structure calculations of metal-binding sites in clusters originating from human metallothionein-2. All possible clusters arising from fully loaded clusters with any combination of Zn^{2+} and Cd^{2+} have been investigated, with the purpose of understanding whether any distinct geometric features and properties occur already intrinsically (*i.e.* before the addition of any protein) in these fascinating inorganic clusters.

From optimized geometries and computed free energies, the most stable isomers have been identified, and the most stable distribution of the seven metal ions within the protein has been predicted at various Cd^{2+} load. Given the accuracy of the procedure (~0.03 Å in bond lengths and ~10 kJ/mol in relative free energies), a number of results have been obtained:

(1) due to the asymmetry of cluster architectures, all seven metal sites are distinct;

(2) the non-strained bond lengths of the tetrathiolate clusters were computed to be 2.60 Å and 2.39 Å, respectively, for Cd–S and Zn–S;

(3) in the clusters, four characteristic bond lengths are observed, depending on metal ion type and whether the sulfur is terminal (t) or bridging (b). The average equilibrium bond lengths are: 2.55 Å ($Cd–S^t$); 2.35 Å ($Zn–S^t$); 2.62 Å ($Cd–S^b$); and 2.42 Å ($Zn–S^b$), which are thus distributed around the non-strained bond lengths. Terminal bonds are 0.07 Å shorter bridging bonds for both Zn and Cd, and correspondingly stronger as shown from the bond orders;

(4) the four possible bonds, $Cd–S^t$, $Zn–S^t$, $Cd–S^b$, and $Zn–S^b$ are of similar length in both the A and B clusters. Thus, no cluster-specific strain is apparent from the metal–ligand bond lengths;

(5) for each stoichiometry of Zn^{2+} and Cd^{2+}, all possible isomers have been characterized and ranked according to relative free energy and the most stable identified;

(6) no correlation between stability and angular structural distortion of the sites is observed;

(7) specific sites display substantial metal ion selectivity: site 380 in cluster A selectively prefers Cd^{2+}, with other sites being more or less neutral to Zn^{2+}/Cd^{2+} differentiation. In cluster B, site 378 has larger selectivity for Cd^{2+}, and 376 has larger selectivity for Zn^{2+};

(8) the most stable distribution in clusters at low Cd^{2+} concentration is computed to be $Zn_4 + CdZn_2$, where the Cd^{2+} is situated at position 378 in Cluster B; this agrees with data by Li and Otvos for Ag^+ and Cu^+;[71]

(9) at 2 : 1 $Cd^{2+} : Zn^{2+}$ concentration, only heteroclusters are thermodynamically stable, explaining experimental data.[35,68] We have identified which individual isomers occur. The driving force for this preference is enthalpic and can be explained from electrostatic consideration of the thiolate positions.

(10) when Cd^{2+} ions are present, angular distortion of the pseudo-tetrahedral sites tend to increase; the native Zn^{2+} sites are less angularly distorted.

Why do MTs consists of two highly asymmetric clusters, compared to the almost tetrahedral clusters made synthetically? This answer must reside already in the intrinsic differences of the two clusters and not merely in the protein scaffold, and answering this question was a key objective of this work. Our current explanation is that asymmetry already inherent in the two different cluster types causes different metal ion affinities of individual sites. This may allow Zn^{2+} transfer to the various molecular targets having different thresholds for Zn^{2+} binding. Furthermore, it allows MTs to maintain dual function by having a primary detoxification site (cluster B) and a primary Zn^{2+} transfer site (cluster A), as suggested by Li and Otvos[71] and shown here to arise already in the inherent cluster differences, *i.e.* without protein present. Having a metal storage and transfer protein which can at the same time dispose of any unwanted and potentially harmful competing heavy metals may have been a substantial evolutionary advantage in the development of the earliest two-subunit MT structures.

Acknowledgements

The authors acknowledge a Steno Fellowship from the Danish Natural Science Research Council, 272-08-0041 (KPJ), and computer time from the Danish Center for Scientific Computing, CPU-0107-05 (KPJ).

References

1 J. H. R. Kagi and B. L. Vallee, *J. Biol. Chem.*, 1960, **235**, 3460–3465.
2 M. Margoshes and B. L. Vallee, *J. Am. Chem. Soc.*, 1957, **79**, 4813–4814.
3 M. J. Vasak, *J. Trace Elem. Med. Biol.*, 2005, **19**, 13–17.
4 Y. Li and W. Maret, *J. Anal. At. Spectrom.*, 2008, **23**, 1055–1062.
5 C. A. Blindauer and P. J. Sadler, *Acc. Chem. Res.*, 2005, **38**, 62–69.
6 M. J. Stillman, C. F. Shaw, III, and K. T. Suzuki, in: *Metallothioneins*, ed. M. J. Stillman, C. F. Shaw, III, K. T. Suzuki, VCH Publishers, New York, 1992, p. 1.
7 M. Penkowa, S. Florit, M. Giralt, A. Quintana, A. Molinero, J. Carrasco and J. Hidalgo, *J. Neurosci. Res.*, 2005, **79**, 522–534.
8 J. H. R. Kagi and A. Schaffer, *Biochemistry*, 1988, **27**, 8509–8515.
9 R. J. Cousins, J. P. Liuzzi and L. A. Lichten, *J. Biol. Chem.*, 2006, **281**, 24085–24089.
10 W. Maret, C. Jacob, B. L. Vallee and E. H. Fischer, *Proc. Natl. Acad. Sci. U. S. A.*, 1999, **96**, 1936–1940.
11 L. J. Jiang, W. Maret and B. L. Vallee, *Proc. Natl. Acad. Sci. U. S. A.*, 1998, **95**, 3483–3488.
12 J. Zeng, R. Heuchel, W. Schaffner and J. H. R. Kägi, *FEBS Lett.*, 1991, **279**, 310–312.
13 J. Zeng, B. L. Vallee and J. H. R. Kägi, *Proc. Natl. Acad. Sci. U. S. A.*, 1991, **88**, 9984–9988.
14 B. K. Y. Bitanihirwe and M. G. Cunningham, *Synapse*, 2009, **63**, 1029–1049.

15 E. Mocchegiani, C. Bertoni-Freddari, F. Marcellini and M. Malavolta, *Prog. Neurobiol.*, 2005, **75**, 367–390.
16 S. L. Sensi, P. Paoletti, A. I. Bush and I. Sekler, *Nat. Rev. Neurosci.*, 2009, **10**, 780–791.
17 A. H. Robbins, D. E. McRee, M. Williamson, S. A. Collett, N. H. Xuong, W. F. Furey, B. C. Wang and C. D. Stout, *J. Mol. Biol.*, 1991, **221**, 1269–1293.
18 B. A. Messerle, A. Schaffer, M. Vasak, J. H. R. Kagi and K. Wuthrich, *J. Mol. Biol.*, 1992, **225**, 433–443.
19 W. F. Furey, A. H. Robbins, L. L. Clancy, D. R. Winge, B. C. Wang and C. D. Stout, *Science*, 1986, **231**, 704–710.
20 G. Henkel and B. Krebs, *Chem. Rev.*, 2004, **104**, 801–824.
21 A. Arseniev, P. Schultze, E. Worgotter, W. Braun, G. Wagner, M. Vasak, J. H. R. Kagi and K. Wuthrich, *J. Mol. Biol.*, 1988, **201**, 637–657.
22 C. Ruiz and A. R. Rodriguez, *Anal. Chim. Acta*, 1997, **350**, 305–317.
23 T. Simonson and N. Calimet, *Proteins: Struct., Funct., Genet.*, 2002, **49**, 37–48.
24 M. G. Cherian and R. A. Goyer, *Life Sci.*, 1978, **23**, 1–10.
25 M. G. Cherian, *Environ. Health Perspect.*, 1984, **54**, 243–248 .
26 J. Chan, Z. Huang, M. E. Merrifield, M. T. Salgado and M. J. Stillman, *Coord. Chem. Rev.*, 2002, **233–234**, 319–339.
27 B. A. Messerle, A. Schaffer, M. Vasak, J. H. R. Kagi and K. Wuthrich, *J. Mol. Biol.*, 1990, **214**, 765–779.
28 N. Romero-Isart and M. Vasak, *J. Inorg. Biochem.*, 2002, **88**, 388–396.
29 T. T. Ngu and M. J. Stillman, *IUBMB Life*, 2009, **61**, 438–446.
30 D. E. K. Sutherland and M. J. Stillman, *Biochem. Biophys. Res. Commun.*, 2008, **372**, 840–844.
31 A. Krezel and W. Maret, *Biochem. J.*, 2007, **402**, 551–558.
32 A. Krezel and W. Maret, *J. Am. Chem. Soc.*, 2007, **129**, 10911–10921.
33 J. D. Otvos, X. Liu, H. Li, G. Shen, and M. Basti, in: *Metallothionein III*, ed. K. T. Suzuki, N. Imura, and M. Kimura, Birkhauser, Basel, 1993, pp. 57-74.
34 J. D. Otvos, D. H. Petering and C. F. Shaw, *Comments Inorg. Chem.*, 1989, **9**, 1–35.
35 D. G. Nettesheim, H. R. Engeseth and J. D. Otvos, *Biochemistry*, 1985, **24**, 6744–6751.
36 L. Zhang, I. J. Pickering, D. R. Winge and G. N. George, *Chem. Biodiversity*, 2008, **5**, 2042–2048.
37 G. Yalovega, G. Smolentsev, A. Soldatov, J. Chan and M. Stillman, *Nucl. Instrum. Methods Phys. Res., Sect. A*, 2007, **575**, 162–164.
38 F.-Y. Ni, B. Cai, Z.-C. Ding, F. Zheng, M.-J. Zhang, H.-M. Wu, H.-Z. Sun and Z.-X. Huang, *Proteins: Struct., Funct., Bioinf.*, 2007, **68**, 255–266.
39 K. P. Jensen, B. O. Roos and U. Ryde, *J. Chem. Phys.*, 2007, **126**, 014103.
40 K. P. Jensen, *Inorg. Chem.*, 2008, **47**, 10357–10365.
41 K. P. Jensen, *J. Phys. Chem. A*, 2009, **113**, 10133–10141.
42 R. Ahlrichs, M. Bär, M. Häser, H. Horn and C. Kölmel, *Chem. Phys. Lett.*, 1989, **162**, 165–169.
43 A. D. Becke, *Phys. Rev. A: At., Mol., Opt. Phys.*, 1988, **38**, 3098–3100.
44 J. P. Perdew, *Phys. Rev. B: Condens. Matter*, 1986, **33**, 8822–8824.
45 A. Schafer, H. Horn and R. Ahlrichs, *J. Chem. Phys.*, 1992, **97**, 2571–2577.
46 A. Klamt and G. J. Schüürmann, *J. Chem. Soc., Perkin Trans. 2*, 1993, 799–805.
47 A. Schafer, A. Klamt, D. Sattel, J. C. W. Lohrenz and F. Eckert, *Phys. Chem. Chem. Phys.*, 2000, **2**, 2187–2193.
48 B. Honig and A. Nicholls, *Science*, 1995, **268**, 1144–1149.
49 K. P. Jensen, *J. Inorg. Biochem.*, 2008, **102**, 87–100.
50 F. Weigend and R. Ahlrichs, *Phys. Chem. Chem. Phys.*, 2005, **7**, 3297–3305.
51 J. P. Perdew, J. Tao, V. N. Staroverov and G. E. Scuseria, *J. Chem. Phys.*, 2004, **120**, 6898–6911.
52 V. N. Staroverov, G. E. Scuseria, J. Tao and J. P. Perdew, *J. Chem. Phys.*, 2003, **119**, 12129–12137.
53 F. Furche and J. P. Perdew, *J. Chem. Phys.*, 2006, **124**, 044103.
54 P. E. M. Siegbahn and M. R. A. Blomberg, *Chem. Rev.*, 2000, **100**, 421–437.
55 A. Silver, S. A. Koch and M. Millar, *Inorg. Chim. Acta*, 1993, **205**, 9–14.
56 J. Otto, I. Jolk, T. Viland, R. Wonnemann and B. Krebs, *Inorg. Chim. Acta*, 1999, **285**, 262–268.
57 I. L. Abrahams and C. D. Garner, *J. Am. Chem. Soc.*, 1985, **107**, 4596–4597.
58 Z. Gui, A. R. Green, M. Kasrai, G. M. Bancroft and M. J. Stillman, *Inorg. Chem.*, 1996, **35**, 6520–6529.
59 U. Ryde and K. Nilsson, *J. Am. Chem. Soc.*, 2003, **125**, 14232–14233.
60 A. Krezel and W. Maret, *JBIC, J. Biol. Inorg. Chem.*, 2008, **13**, 401–409.
61 W. Feng, J. Cai, W. M. Pierce, R. B. Franklin, W. Maret, F. W. Benz and Y. J. Kang, *Biochem. Biophys. Res. Commun.*, 2005, **332**, 853–858.
62 M. Sato and I. Bremner, *Free Radical Biol. Med.*, 1993, **14**, 325–337.
63 A. Unkiewicz-Winiarczyk, K. Gromysz-Kalkowska and E. Szubartowska, *Biol. Trace Elem. Res.*, 2009, **132**, 41–50.
64 N. K. Wills, V. M. S. Ramanujam, J. Chang, N. Kalariya, J. R. Lewis, T.-X. Weng and F. J. G. M. Van Kuijk, *Exp. Eye Res.*, 2008, **86**, 41–51.
65 L. Jarup and A. Akesson, *Toxicol. Appl. Pharmacol.*, 2009, **238**, 201–208.
66 M. J. Stillman, *Coord. Chem. Rev.*, 1995, **144**, 461–511.
67 J. D. Otvos, R. W. Olafson and I. M. Armitage, *J. Biol. Chem.*, 1982, **257**, 2427–2431.
68 M. Good, R. Hollenstein and M. Vasak, *Eur. J. Biochem.*, 1991, **197**, 655–659.
69 K. Zangger, G. Oz, E. Haslinger, O. Kunert and I. M. Armitage, *FASEB J*, 2001, **15**, 1303–1305.
70 K. S. Hagen, W. D. Stephan and R. H. Holm, *Inorg. Chem.*, 1982, **21**, 3928–3936.
71 H. Li and J. D. Otvos, *J. Inorg. Biochem.*, 1998, **70**, 187–194.
72 K. B. Nielson and D. R. Winge, *J. Biol. Chem.*, 1983, **258**, 13063–13069.
73 C. Jacob, W. Maret and B. L. Vallee, *Proc. Natl. Acad. Sci. U. S. A.*, 1998, **95**, 3489–3494.